Genes Involved in Energy Metabolism Are Differentially Expressed During the Day–Night Cycle in Murine Retinal Pigment Epithelium

Elja M. M. Louer,[1,2] Guoqiang Yi,[3] Claudia Carmone,[1] Joris Robben,[1] Henk G. Stunnenberg,[3] Anneke I. den Hollander,[2,4] and Peter M. T. Deen[1]

[1]Department of Physiology, Radboud Institute for Molecular Life Sciences, Radboud University Medical Center, Nijmegen, The Netherlands
[2]Department of Ophthalmology, Donders Institute of Brain, Cognition and Behaviour, Radboud University Medical Center, Nijmegen, The Netherlands
[3]Department of Molecular Biology, Radboud Institute for Molecular Life Sciences, Radboud University Nijmegen, Nijmegen, The Netherlands
[4]Department of Human Genetics, Donders Institute for Brain, Cognition and Behaviour, Radboud University Medical Center, Nijmegen, The Netherlands

Correspondence: Anneke I. den Hollander, Department of Ophthalmology, Radboud University Medical Center, P.O. Box 9101, 6500 HB, Nijmegen, The Netherlands; anneke.denhollander@radboudumc.nl. Peter M.T. Deen, Radboud University Medical Center, P.O. Box 9101, 6500 HB, Nijmegen, The Netherlands; peterdeen11@gmail.com.

Received: September 11, 2019
Accepted: February 15, 2020
Published: May 27, 2020

Citation: Louer EMM, Yi G, Carmone C, et al. Genes involved in energy metabolism are differentially expressed during the day–night cycle in murine retinal pigment epithelium. *Invest Ophthalmol Vis Sci.* 2020;61(5):49. https://doi.org/10.1167/iovs.61.5.49

Purpose. The functional interaction between photoreceptors and retinal pigment epithelium (RPE) cells is essential for vision. Phagocytosis of photoreceptor outer segments (POSs) by the RPE follows a circadian pattern; however, it remains unknown whether other RPE processes follow a daily rhythm. Therefore, our aim was to identify RPE processes following a daily rhythm.

Methods. Murine RPE was isolated at Zeitgeber time (ZT) 0, 2, 4, 9, 14, and 19 (n = 5 per time point), after which RNA was isolated and sequenced. Genes with a significant difference in expression between time points ($P < 0.05$) were subjected to EnrichR pathway analysis to identify daily rhythmic processes.

Results. Pathway enrichment revealed 13 significantly enriched KEGG pathways ($P < 0.01$), including the metabolic pathway ($P = 0.002821$). Analysis of the metabolic pathway differentially expressed genes revealed that genes involved in adenosine triphosphate production, glycolysis, glycogenolysis, and glycerophospholipid were low at ZT0 (light onset) and high at ZT19 (night). Genes involved in fatty acid degradation and cholesterol synthesis were high at light onset and low at night.

Conclusions. Our transcriptome data suggest that the highest energy demand of RPE cells is at night, whereas POS phagocytosis and degradation take place in the morning. Furthermore, we identified genes involved in fatty acid and glycerophospholipid synthesis that are upregulated at night, possibly playing a role in generating building blocks for membrane synthesis.

Keywords: retinal pigment epithelium, metabolism, RNA-sequencing, circadian rhythm, day–night cycle

Vision is a complex process in which different cell layers of the retina functionally interact. The retina consists of supporting cells, neuronal (bipolar and ganglion) cells, photoreceptor (PR) cells, and retinal pigment epithelium (RPE) cells. The RPE, which is a monolayer of hexagonal, highly pigmented cells adjacent to the photoreceptor outer segment (POS) side of PR cells, plays an important role in the maintenance of the PR cells. This cell layer is responsible for the removal of PR cell waste products,[1,2] for phagocytosis and degradation of shed POS membranes,[3] and for regeneration of 11-*cis*-retinal from 11-*trans*-retinal and subsequent recycling to PR cells.[4,5] Phagocytosis of POSs provides RPE cells with a high load of (lipo)proteins, (oxidized) lipids, and 11-*trans*-retinal.[6–9] In vitro cell culture studies have shown that RPE cells degrade phagocytosed lipids to fatty acids (FAs) and subsequently subject them to β-oxidation to be used in the tricarboxylic acid (TCA) cycle to provide these cells with adenosine triphosphate (ATP).[10,11]

The activity of many processes in PR cells and POS binding and subsequent phagocytosis by the RPE follow a circadian rhythm, with a peak in phagocytic activity in the morning, around 2 hours after light onset, or Zeitgeber time 2 (ZT2).[12–15] It is likely that several other RPE processes follow a circadian rhythm, but these are yet unknown. In addition to the physiological value, knowledge of such pathways may also be of clinical relevance, because a dysfunctional RPE underlies age-related macular degeneration (AMD). Of particular interest here is the

metabolic pathway, because oxidative stress and the generation of reactive oxygen species have been recognized as important factors contributing to aging and age-related disorders, including AMD.[16,17] Therefore, the aim of our study was to identify RPE processes that show a daily rhythm, with a particular focus on the metabolic pathway.

Methods

Eye Isolation and Dissection

C57BL/6NCrl wild-type mice were housed under standardized conditions (12-hour dark/12-hour light cycle) and fed ad libitum. Animal experiments were approved by the animal ethics board of Radboud University, Nijmegen (RU DEC 2016-0054) and by the Dutch Central Commission for Animal Experiments (AVD1030002016620). All animal handling and procedures were performed according to the ARVO Statement for the Use of Animals in Ophthalmic and Vision Research.

For RNA-sequencing (RNA-seq) analysis, 10- to 13-week-old male mice were randomly distributed over six time points (ZT0, ZT2, ZT4, ZT9, ZT14, and ZT19). At each time point, mice were sacrificed using cervical dislocation, and the eyes were collected via enucleation (n = 5 mice per time point). Anterior segments (cornea, iris, and lens) were removed to expose the posterior eyecup. The retina was carefully peeled off, and the eyecup containing the RPE, sclera, and choroid were stored in RNA*later* solution (Thermo Fisher Scientific, Waltham, MA, USA) within 10 minutes after enucleation. The tissue was stored for 2 weeks at –20°C prior to RNA isolation.

RPE RNA Isolation

For RNA isolation, the RPE was removed gently from the choroidal layer using fine forceps. The brown clumps of RPE cells were dissolved in RLT Buffer from the RNeasy Micro Kit (Qiagen, Hilden, Germany). RNA was extracted with the RNeasy Micro Kit according to the manufacturer's protocol using the on-column DNase treatment. The RNA concentration and quality were measured using a NanoDrop 2000c spectrophotometer (Thermo Fisher Scientific).

RNA-Sequencing

RNA samples of one eye per mouse, five mice per time point, were sent to ServiceXS (GenomeScan, Leiden, The Netherlands) for sequencing. The RNA concentrations and RNA quality number scores (Supplementary Table S1) were assessed using the Advanced Analytical Fragment Analyzer (Agilent Technologies, Santa Clara, CA, USA) prior to library construction. Library preparation was performed using the NEBNext Ultra Directional RNA Library Prep Kit for Illumina (New England Biolabs, Ipswich, MA, USA). We used 1.6 pM of cDNA for input samples in the Illumina NextSeq 500 sequencer (San Diego, CA, USA) for 1 × 75-bp single-read sequencing, sequencing an average of 20 million reads per sample.

Quality Control of RNA-Sequencing Data

The mm10 reference assembly was first indexed by STAR mapper[18] with a gene annotation model from the ENSEMBL database. The RNA-seq reads were aligned to the mm10 genome using the two-pass mode of STAR, and the gene-based read counts were quantified at the same time.

To evaluate the purity of cellular population and to expose cell-type signature genes in our bulk samples, the CIBERSORT (Cell type Identification by Estimating Relative Subsets of Known RNA Transcripts) method[19] was applied based on gene expression data. In order to generate a matrix of reference gene expression signatures, we downloaded expression values derived from 44k Agilent microarrays (Santa Clara, CA, USA), under GSE66916 accession,[20] comprised of RPE, PR, and choriocapillaris cells isolated by laser dissection microscopy and excision from mouse eyes at high purity. Then, the fragments per kilobase per million mapped reads (FPKM) value for each gene was used as input for CIBERSORT with default parameters, except for the use of 1000 permutation tests.

Analysis of RNA-Sequencing Data for Differentially Expressed Genes

The DESeq2 package[21] was used to detect differentially expressed genes by performing pairwise comparisons among the six described time points. Only genes with a Benjamini–Hochberg-adjusted P value < 0.05 and fold change > 1.5 were considered significantly differentially expressed. Cufflinks[22] was employed to estimate gene-level abundance in FPKM values for ENSEMBL genes. To group those differential genes with similar time-series-based expression patterns, the k-means clustering algorithm was conducted based on z-score normalization and then displayed as a heat map.

Pathway Analysis of Differentially Expressed Genes

KEGG-2016 pathway analysis was performed using the EnrichR software[23,24] (http://amp.pharm.mssm.edu/Enrichr/) and online DAVID (Database for Annotation, Visualization and Integrated Discovery) v6.8 (https://david.ncifcrf.gov/). The EnrichR pathway clustering option was used to identify the overlap between the significantly enriched pathways. WikiPathways were used to generate pathways shown in Figures 4 and 6A using PathVisio software.[25–28]

Data Availability

The RNA-seq data used in this paper have been deposited in the Gene Expression Omnibus database[29] with the accession number GSE137005.

RNA-Sequencing Validation Using Quantitative Real-Time Polymerase Chain Reaction

The RNA-seq dataset was validated using quantitative real-time PCR (qRT-PCR) (Supplementary Fig. S1). Thirteen genes with a fold change above 1.5 were selected for validation and represented seven of the eight expression clusters. Reverse transcription was performed using Moloney murine leukemia virus reverse transcriptase (Invitrogen, Carlsbad, CA, USA) according to the manufacturer's protocol. qRT-PCR was performed with the iTAQ Universal SYBR Green

Investigative Ophthalmology & Visual Science

Supermix (Bio-Rad, Hercules, CA, USA) using the CFX Connect Real-Time System (Bio-Rad). *Gusb* expression was used as housekeeping gene. Real-time PCR primers are listed in Supplementary Table S2.

Immunoblot Analysis

Male C57BL/6NCrl wild-type mice 11 weeks old were arbitrarily distributed over four ZT points (ZT0, ZT4, ZT9, and ZT19) at which the eyes were isolated. Three animals were sacrificed per time point. Mice were sacrificed using CO_2, and the eyes were collected via enucleation. Anterior segments were removed, after which each retina was carefully peeled off. The RPE was subsequently mechanically detached and dissolved in lysis buffer, comprised of 10-mM Tris, 150-mM NaCl, 0.5% Triton X-100 (Sigma-Aldrich, St. Louis, MO, USA), and 0.1% sodium dodecyl sulfate (SDS), and cOmplete EDTA-Free Protease Inhibitors (Roche Group, Basel, Switzerland).

The protein concentrations of lysates were determined using a bicinchoninic acid protein assay reagent (Pierce Biotechnology, Rockford, IL, USA) and quantified with a plate reader (Tecan Group AG, Männedorf, Switzerland). Protein lysates were mixed with Laemmli buffer, denatured at 95°C for 5 minutes, separated on precast SDS polyacrylamide gels (4%–20% gradient; Bio-Rad), and blotted onto a polyvinylidene difluoride membrane (PerkinElmer, Boston, MA, USA). The oxidative phosphorylation system (OXPHOS) proteins of interest were detected using the Abcam OXPHOS antibody cocktail for immunoblot (ab110413, dilution 1:250; Cambridge, United Kingdom) and peroxidase-conjugated anti-mouse secondary antibody (1:10,000; Jackson ImmunoResearch Laboratories, West Grove, PA, USA). Proteins were visualized using enhanced chemiluminescence (Pierce Biotechnology). Following Coomassie Brilliant blue staining of the blot, the signals of the proteins of interest and the Coomassie signals were subjected to densitrometric analyses using Bio-Rad quantification equipment (Bio-Rad 690c Densitometer; Chemidoc XRS) and Image Studio software (LI-COR Biosciences, Lincoln, NE, USA). Coomassie blue was used to normalize for protein loading differences. Statistical analyses were performed using GraphPad Prism 5 software. One-way ANOVA with repeated measures, followed by Bonferroni post hoc tests, were used. $P < 0.05$ was considered significant.

Results

Generation of a Diurnal Transcriptome of Murine RPE

To identify daily rhythms in gene expression in RPE cells, mouse eyes were dissected at six ZT points (ZT0, ZT2, ZT4, ZT9, ZT14, and ZT19) (Fig. 1A). Because the peak time point in the phagocytosis of POSs by RPE cells was known to occur around ZT2[12] (Fig. 1A, indicated with an arrow), we selected three time points (ZT0, ZT2, and ZT4) around this peak and distributed the other three time points evenly over the remaining 20 hours. To determine the purity of our RPE preparations, we compared our RNA-seq data to the data of RPE, PR, and choriocapillaris cells isolated by laser dissection microscopy and excision in a previous study.[20] Based on the RNA-seq data, all of our samples appeared highly enriched for RPE, as 70% of the reads were of RPE origin with only limited contamination of neighboring PR and choroidal endothelial cells (Supplementary Fig. S2). This allowed us to use our RNA-seq data to study the physiology of RPE cells.

Identification of Genes Expressed Differentially Over Time

Pairwise comparison of the six ZT points resulted in a total of 756 unique differentially expressed genes (DEGs) with a Benjamini–Hochberg-adjusted $P < 0.05$ (Fig. 1B). Limited or no differences were observed among ZT0, ZT2, and ZT4, indicating that the mRNA expression patterns of these ZT points were highly similar to each other. The highest number of transcriptome differences was observed between ZT0 and ZT19, which yielded 618 DEGs. Overall, the highest number of DEGs was observed comparing ZT19 to all other ZT points, except for ZT4. This comparison resulted in only nine DEGs. Thirteen DEGs were selected to validate our RNA-seq dataset using qRT-PCR (Supplementary Fig. S1). A detailed list of DEGs identified in each pairwise comparison of ZT points is provided in Supplementary Table S3. To study the expression pattern of the identified DEGs over time, DEGs with similar expression patterns were clustered using a *k*-means algorithm. In total, eight different clusters were identified, each showing a unique expression pattern over time (Fig. 1C).

Pathway Analysis of Identified DEGs

Subsequent analysis of the 756 DEGs using the EnrichR pathway software revealed 13 significantly enriched KEGG pathways (adjusted $P < 0.01$) (Table). Similar pathways were identified using the DAVID pathway analysis tool (Supplementary Table S4). More detailed cluster analysis of the top 10 KEGG pathways using the cluster option from EnrichR resulted in three main groups of pathways having multiple genes in common: (1) circadian rhythm, (2) Alzheimer's disease and metabolic pathways, and (3) a diverse set of remaining processes (Table). The circadian rhythm group contained nine genes, the Alzheimer's disease and metabolic pathways group contained 81 genes, and the third group contained 55 genes (Fig. 1D). Among these groups, only one gene overlapped between groups 1 and 3 (*Prkab2*) and one gene overlapped between groups 2 and 3 (*Cacna1s*). Identification of the circadian rhythm pathway (Fig. 2) confirms proper isolation of the material at the different time points. The expression pattern and timing of these genes at different ZTs are similar to those previously described for several organs such as the hypothalamus, liver, kidney, and heart.[30]

Day–Night Rhythm of Metabolic Pathway Genes

Next, a more detailed analysis was performed for the 73 DEGs overlapping with the metabolic pathway (Table). Figure 3 shows the *z*-score transformed expression data for each gene. We examined in detail the metabolic pathways to which each gene belonged and determined whether the genes in these pathways had similar expression patterns.

Nine genes encoding for building blocks of the mitochondrial electron transport chain (ETC) were found to be highly expressed at ZT19 (*Ndufa6*, *Ndufc1*, *Ndufs2*, *Sdhb*, *Uqcrq*, *Cox5a*, *Cox5b*, *Cox7b*, and *Atp5c1*) (Fig. 4A). In addition, seven other genes (*mt-Nd1*, *mt-Nd2*, *mt-Nd4*,

Investigative Ophthalmology & Visual Science

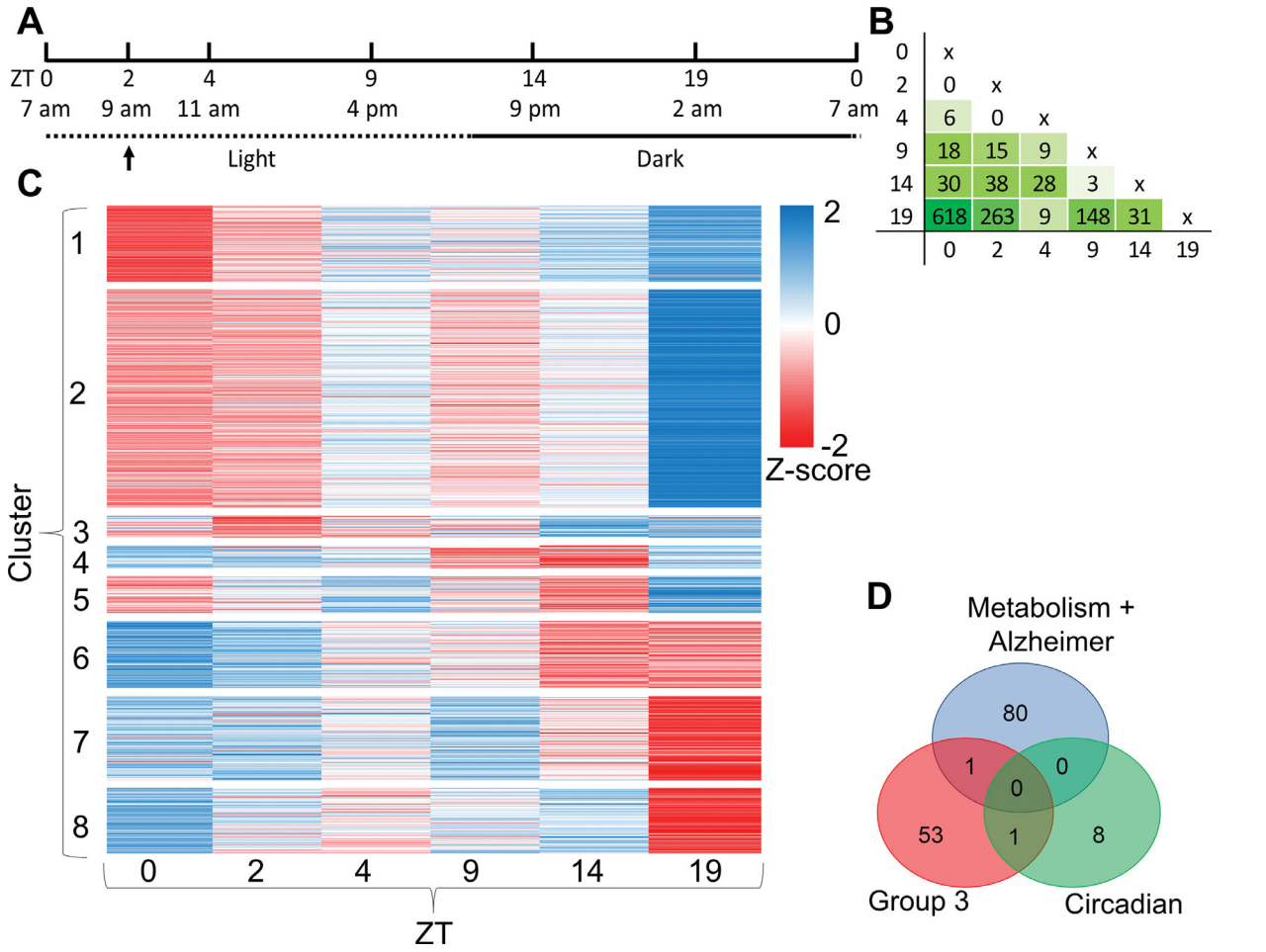

Figure 1. Circadian expression of RPE genes. (**A**) The experimental setup showing the time points chosen for tissue harvesting indicated in both real and Zeitgeber time (ZT). The arrow indicates peak phagocytic activity. (**B**) Number of DEGs identified among the different time points, which are indicated in ZT. (**C**) Heat map of DEGs. To group the DEGs with similar time-based expression patterns, *k*-means clustering was conducted based on *z*-score normalization. The intensity scale of the standardized expression values ranges from low expression (*dark blue*) to high expression (*dark red*). (**D**) Venn diagrams showing the number of DEGs overlapping among groups, as identified by EnrichR string analysis.

Table. Significant KEGG Pathway Enrichment Using EnrichR Pathway Analysis

Term	DEGs, n	Adjusted *P* Value (*P* < 0.01)	String Analysis Group
Tight junction (hsa04530)	22	3E-06	Group 3
Circadian rhythm (hsa04710)	9	0.000125	Group 1
Alzheimer's disease (hsa05010)	21	0.000125	Group 2
Arrhythmogenic right ventricular cardiomyopathy (hsa05412)	13	0.00022	Group 3
Leukocyte transendothelial migration (hsa04670)	15	0.00189	Group 3
Regulation of actin cytoskeleton (hsa04810)	21	0.002273	Group 3
Hypertrophic cardiomyopathy (hsa05410)	12	0.002273	Group 3
Metabolic pathways (hsa01100)	73	0.002821	Group 2
Adherens junction (hsa04520)	11	0.002821	Group 3
Dilated cardiomyopathy (hsa05414)	12	0.003489	Group 3
Cardiac muscle contraction (hsa04260)	11	0.003592	—
Parkinson's disease (hsa05012)	15	0.006463	—
Calcium signaling pathway (hsa04020)	17	0.009249	—

The number of DEGs found in our dataset that overlap with the reference pathways and *P* values are indicated. The *P* values indicate the significance of enrichment and were Benjamini corrected. Groups identified using EnrichR string analysis are indicated.

Investigative Ophthalmology & Visual Science

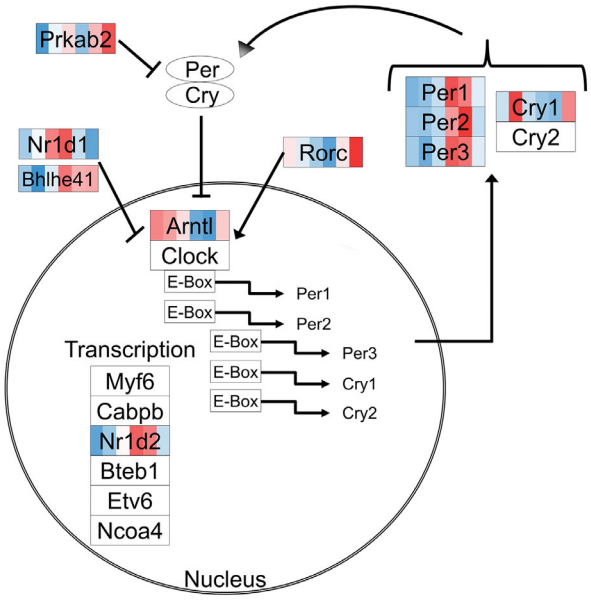

Figure 2. DEGs in RPE cells of the circadian rhythm pathway. Genes that are differentially expressed over time are indicated by various colors, with an intensity scale of the standardized expression values ranging from low expression (*dark blue*) to high expression (*dark red*). ZT points are ranked from left to right for each differentially expressed gene, the most left color corresponding to ZT0 and the most right color corresponding to ZT19.

Cytb, *mt-Co1*, *Cox7a1*, and *Slc25a4*) encoding components of the mitochondrial ETC were identified as DEGs in our RNA-seq dataset and were also expressed highly at ZT19 (Fig. 4A). Furthermore, we identified two genes (*Ckm* and *Ak1*) involved in facilitating transport of ATP among the DEGs in the metabolic pathway and two additional ATP transport genes (*Ckmt1* and *Ckmt2*) in the entire list of DEGs.

To verify whether protein levels corresponded to changes in the RNA levels, we subjected proteins of isolated RPE to immunoblot analysis for the OXPHOS proteins Ndufb8, Sdhb, Uqcrc2, mt-Co1, and Atp5a, which are subunits of mitochondrial ETC complexes I to V, respectively. Of these OXPHOS proteins, Ndufb8, Sdhb, and mt-Co1 represent DEGs. A trend for increased expression at ZT19 and ZT0 was observed for all complexes, except for complex V subunit Atp5a, which did not have increased expression at ZT19 (Fig. 5).

Among the DEGs in the metabolic pathway, three genes of the TCA cycle (*Idh3a*, *Sdhb*, and *Pdhb*) were identified, all showing a high expression at ZT19 (Fig. 4B). *Idh3a* encodes the isocitrate dehydrogenase α-subunit of the mitochondrial Idh3 complex, which catalyzes the rate-limiting step in the TCA cycle.[31]

The production of ATP requires an energy source, typically in the form of carbohydrates or FAs.[32] Three genes involved in glucose metabolism (*Pfkm*, *Eno3*, and *Got1*) were identified among the DEGs in the metabolic pathway, and further analysis identified *Slc2a4* as an additional DEG in our RNA-seq dataset, all having high expression at ZT19 (Fig. 6A). *Pfkm* encodes 6-phosphofructrokinase, muscle type, which has unidirectional activity as it drives glycolysis instead of gluconeogenesis. Furthermore, *Pdhb* codes for pyruvate dehydrogenase, which links glycolysis to the TCA cycle as it catalyzes the irreversible conversion of

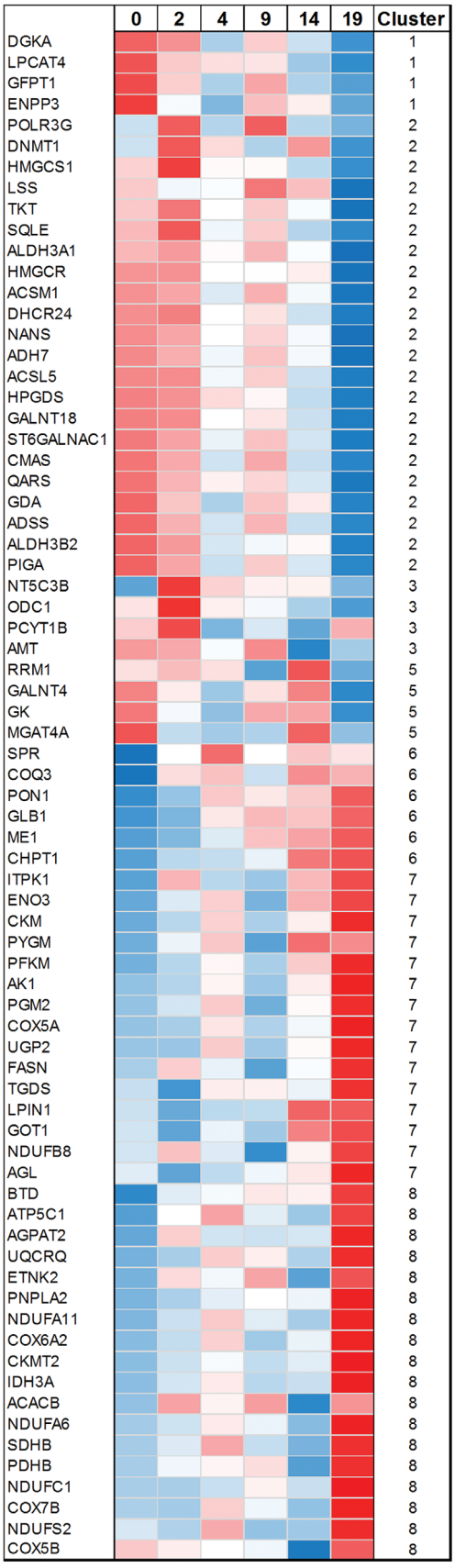

Figure 3. Heat map of differentially expressed genes overlapping with the metabolic pathway. The normalized expression data were converted to heat map colors using a *z*-score transformation for each gene. The intensity scale of the standardized expression values ranges from low expression (*dark blue*) to high expression (*dark red*). Gene names, ZT points, and clusters are indicated.

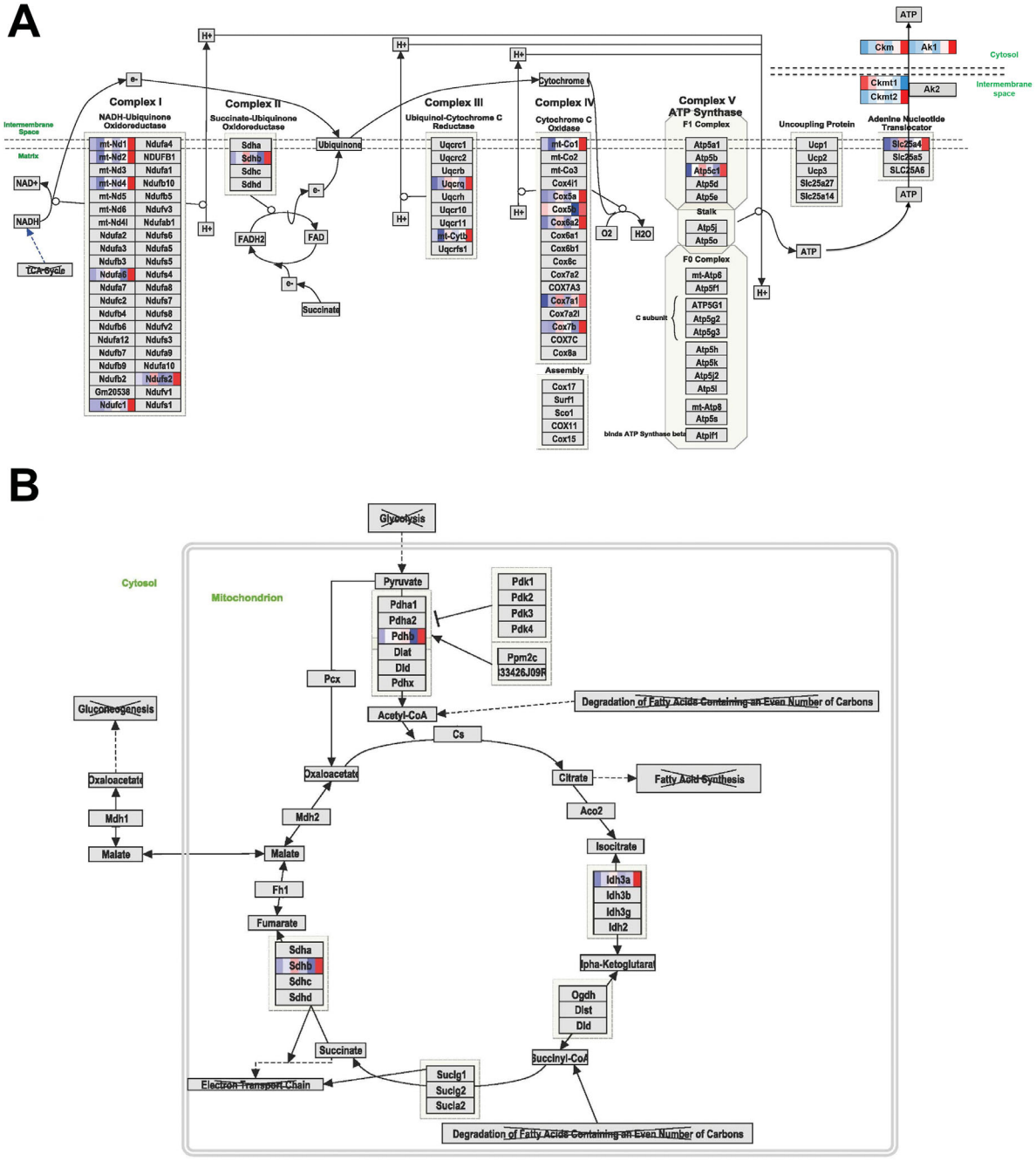

Figure 4. DEGs in RPE cells of ATP-producing pathways. Shown are the detailed WikiPathways of the protein (complexes) involved in the mitochondrial ETC (**A**) and glycolysis (**B**). Genes differentially expressed over time are indicated with colors, with an intensity scale of the standardized expression values ranging from low expression (*dark blue*) to high expression (*dark red*). ZT points are ranked from left to right for each DEG, the most left color corresponding to ZT0 and the most right color corresponding to ZT19. Links to other pathways are indicated by the name of the pathway with a cross.

pyruvate to acetyl-CoA.[33] *Pdhb* also showed high expression at ZT19 (Fig. 4B).

Additionally, four genes involved in glycogen metabolism were identified in the metabolic pathway (*Agl*, *Pygm*, *Pgm2*, and *Ugp2*), and detailed analysis of DEGs in our RNA-seq dataset identified three additional genes (*Gys1*, *Phka1*, and *Phkg1*) involved in glycogen metabolism. Again, all DEGs showed a high expression at ZT19, suggesting conversion of glycogen to glucose at this time point (Fig. 6B).

Glycerophospholipid metabolism genes were also represented in the list of DEGs overlapping with the metabolic pathway (*Gk1*, *Agpat2*, *Lpin1*, *Dgka*, *Pnpla2*, *Lpcat4*, *Chpt*, *Pcyt1b*, *Etnk2*, *Acacb*, and *Fasn*), and additional analysis revealed that *Gpd1* and *Btb* were also identified as DEGs (Fig. 7). The expression of these genes varies over time, but genes involved in FA synthesis (*Acacb*, *Btd*, and *Fasn*) were found to be high at ZT19.

Four genes involved in FA degradation were found among the DEGs in the metabolic pathway (*Aldh3b2*, *Acsl5, Acsm1*,

Investigative Ophthalmology & Visual Science

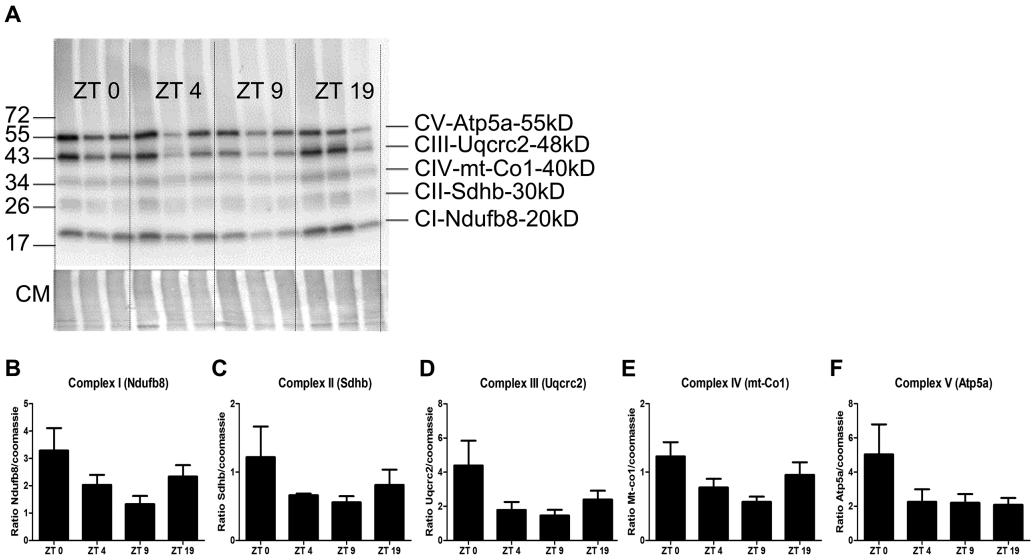

Figure 5. Protein abundance of mitochondrial ETC complexes during the day–night cycle. (**A**) The RPE of each of three mice per time point (ZT0, ZT4, ZT9, and ZT19) was isolated, dissolved, and subjected to immunoblotting for the indicated subunits of the five mitochondrial ETC complexes. Coomassie (CM) staining was used as the loading control and to normalize the signals of the proteins of interest. (**B–F**) Normalized protein quantification for each of the five complexes.

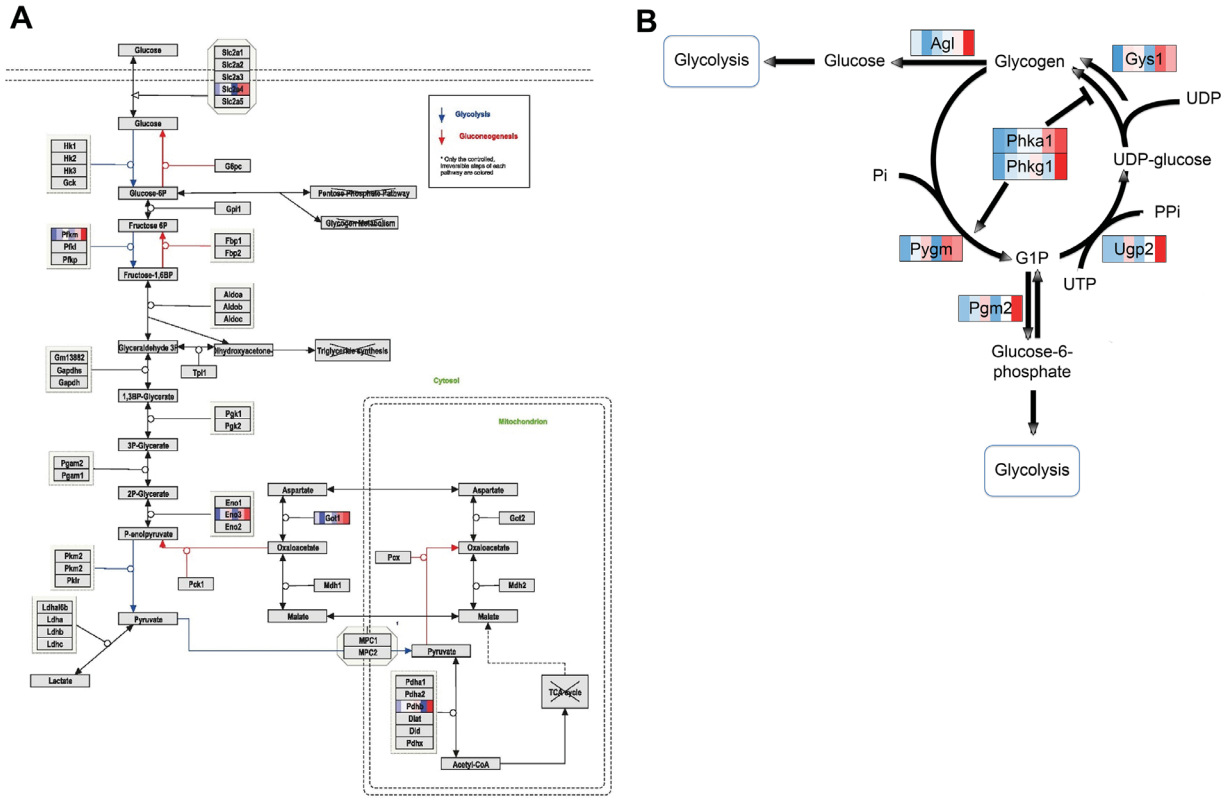

Figure 6. DEGs in RPE cells of the sugar metabolizing pathway. Shown are detailed WikiPathways for glycolysis (**A**) and glycogen metabolism (**B**). Genes differentially expressed over time are indicated by various colors, with an intensity scale of the standardized expression values ranging from low expression (*dark blue*) to high expression (*dark red*). ZT points are ranked from left to right for each DEG, the most left color corresponding to ZT0 and the most right color corresponding to ZT19.

Investigative Ophthalmology & Visual Science

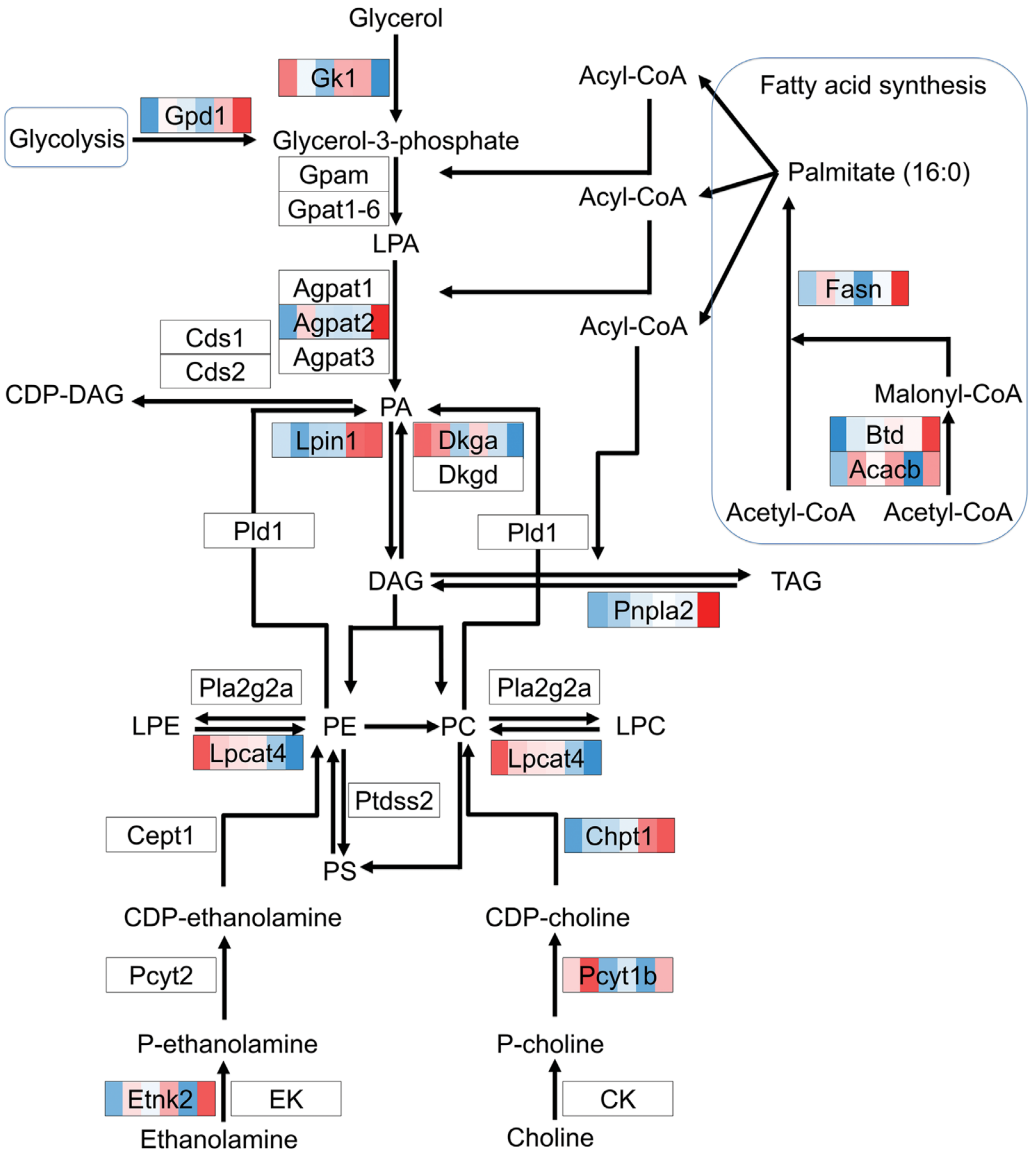

Figure 7. DEGs in RPE cells of the glycerophospholipid metabolism pathway. Genes that are differentially expressed over time are indicated by various colors, with an intensity scale of the standardized expression values ranging from low expression (*dark blue*) to high expression (*dark red*). ZT points are ranked from left to right for each differentially expressed gene, the most left color corresponding to ZT0 and the most right color corresponding to ZT19. DAG, diacylglycerol; LPC, lysophosphatidyl choline; LPE, lysophosphatidyl ethanolamine; PA, phosphatidic acid; PC, phosphatidyl choline; PE, phosphatidyl ethanolamine; TAG, triacylglycerol.

and *Aldh3a1*), as well as five genes involved in cholesterol biosynthesis (*Hmgcs1*, *Hmgcr*, *Sqle*, *Lss*, and *Dhcr24*) (Fig. 8). Of these genes, *Hmgcr* encodes the rate-limiting enzyme for cholesterol synthesis. These genes were all highly expressed at ZT0 and ZT2.

Discussion

In this study, we identified 756 significant DEGs in murine RPE when comparing six different ZT points. Pathway analysis of the DEGs resulted in 13 significantly enriched KEGG pathways, including circadian rhythm and the metabolic pathway. In-depth analysis of the DEGs in the metabolic pathway revealed high expression in the middle of the night (ZT19) of genes involved in the mitochondrial ETC, TCA cycle, glycolysis, and glycogen metabolism, suggesting a greater need for energy production at this time point. Additionally, genes were identified in the glycerophospholipid metabolism pathway, suggesting the generation of glycerophospholipids at ZT19. Finally, genes involved in FA degradation and cholesterol synthesis were observed to be high at light onset and low at night.

In total, we identified 16 genes encoding for building blocks of the mitochondrial ETC, which is involved in ATP production, that were differentially expressed over time but all showed a high expression at ZT19. Furthermore, we identified the main players in the transport of ATP throughout the cell to make it available for ATP-consuming proteins. Maintaining low mitochondrial ATP/adenosine diphosphate (ADP) levels stimulates oxidative phosphorylation and allows high ATP/ADP levels at sites of utilization.[34] Taken together, these observations suggest an

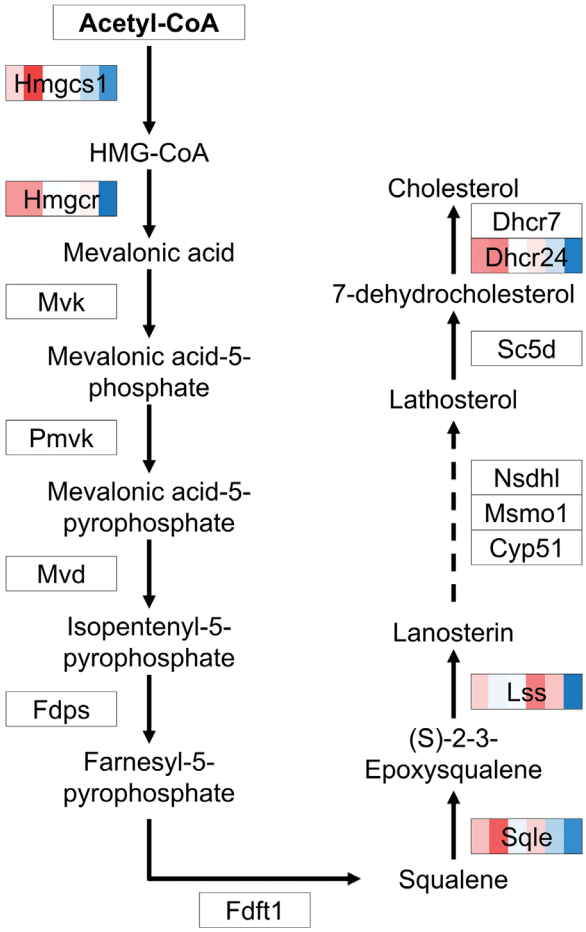

Figure 8. DEGs in RPE cells of the cholesterol synthesis pathway. Genes differentially expressed over time are indicated by various colors, with an intensity scale of the standardized expression values ranging from low expression (*dark blue*) to high expression (*dark red*). ZT points are ranked from left to right for each differentially expressed gene, the most left color corresponding to ZT0 and the most right color corresponding to ZT19.

elevation in the production of ATP in the middle of the night.

Furthermore, we observed a trend in protein abundance of the OXPHOS complexes I to IV, which showed higher levels at ZT0 and ZT19. The RNA expression levels of the corresponding DEGs did not reflect the protein abundance at ZT0, which can be explained by the stability of proteins in the RPE and therefore a delay in translation of RNA levels to protein levels. Because complexes I to IV are responsible for generating the proton gradient driving ATP production by complex V,[35] we hypothesize that ATP production increases at night.

In addition, we identified higher expression at night of genes encoding components of the TCA cycle. This pathway not only generates ATP but is also linked to the ETC in the cellular respiration pathway generating metabolites utilized in the ETC.[32] Our data suggest that the TCA cycle fuels the ETC specifically in the middle of the night.

Although TCA energy can in principle be obtained from carbohydrates, FAs, and amino acids, our data suggest increased glucose and glycogen usage at night. It was surprising to find an elevated expression of genes involved in glycolysis, as it has been reported that RPE cells transport the majority of the glucose they take up from the bloodstream toward the PR cells.[36] However, the increased expression of genes involved in glycogenolysis at night suggests that glucose molecules are generated from glycogen stored in RPE cells at this time point. In previous studies, glycogen was detected in rat and human RPE in vivo, was shown to accumulate in diabetic RPE of rats and humans, and has been shown to be utilized for energy storage in human RPE cells cultured in vitro.[37–39] Our data suggest that glycogen usage shows a daily rhythm and that stored glycogen is metabolized and used as an energy source at night. It remains unclear what process requires this elevation in ATP production. Furthermore, future in vivo metabolic labeling studies on RPE layers must be performed to reveal whether our transcriptomic data are supported by functional metabolic data.

The changes in expression of genes involved in FA synthesis and glycerophospholipid metabolism suggest that the produced FAs are converted to phosphatidyl choline, phosphatidyl ethanolamine, and their lysophosphatidic counterparts at night. The increased expression of *Gpd1* at this time point further suggests that the required glycerol-3-phosphate is derived from the glycolysis pathway, thereby linking the glycolysis pathway to the glycerophospholipid pathway. Glycerophospholipids are building blocks for the generation of biological membranes, and an increase in the synthesis of glycerophospholipids has been associated with phagocytic cells.[40] Because the RPE phagocytoses POSs at the onset of light, the suggested upregulation of phospholipid generation at night could play an important role in this process. Alternatively, the membrane building blocks could be transported to the PR cells for the formation of new POSs.

In addition to genes involved in FA synthesis, we also identified genes involved in FA degradation. These genes had low expression at night (ZT19) but high in the morning (ZT0–ZT2), and they play a role in performing the first steps in targeting FAs for mitochondrial β-oxidation. This suggests reduced energy generation from FAs at night but increased energy generation from FAs in the morning. In the RPE, lipids are degraded and FAs are oxidized by β-oxidation, as shown by in vitro studies.[10,11] β-Oxidation is an important part of FA degradation and takes place in mitochondria, where FAs are processed and acyl-CoA is degraded into acetyl-CoA,[41] after which it can be utilized in the TCA cycle to fuel the mitochondrial ETC. In vitro studies previously demonstrated that RPE cells can use the lipids ingested after POS phagocytosis as an energy source,[42,43] and it has been suggested that they even provide intermediates of the lipid degradation products as building blocks or energy sources for the PR cells.[44,45] Because the ETC is fueled both at night (by TCA and glycolysis) and in the morning (by β-oxidation), this could explain why gene expression levels at ZT4 and ZT19 are relatively similar to each other.

Finally, we identified an increased expression of genes involved in the cholesterol synthesis pathway at light onset. Cholesterol synthesis most likely plays a role during POS phagocytosis in the morning. The PR cells shed their POSs, which are engulfed by the RPE. A fluidic membrane for the engulfment of these POSs is necessary, and the composition of cholesterol and unsaturated free FAs in the membrane is important for membrane fluidity and stability.[46] On the other hand, our study demonstrated that genes involved in FA degradation are upregulated in the morning. The formation of acetyl-CoA from FA degradation can be utilized for the initiation of cholesterol synthesis in the RPE cells. Thus,

Investigative Ophthalmology & Visual Science

cholesterol synthesis and FA degradation are associated with each other, and these pathways most likely work together to facilitate the phagocytosis and breakdown of POSs by the RPE.

The function of the retina, particularly the RPE cells, declines with age.[47] The phagocytosis of POSs contributes to an oxidative environment in the RPE cells,[48] which is believed to contribute to the development of age-related eye disorders such as diabetic retinopathy and AMD.[49] Furthermore, a 30% decrease in intracellular ATP levels was found in aged RPE cells in vitro, mainly due to diminished activity of the ETC.[50,51] This reduced metabolic capacity of aged RPE cells correlates with a high susceptibility to oxidative stress,[52] and reduced mitochondrial function is a hallmark of AMD.[38] Our data suggest that the aged RPE cells might be exposed to high levels of oxidative stress at night due to reduced ATP levels but are exposed to an oxidative environment during POS phagocytosis in the morning. Because RPE cells have many physiological functions, reduced metabolic capacity and increased oxidative stress could lead to cellular dysfunction and, in turn, to retinal pathologies.

In conclusion, our study demonstrates that genes involved in or linked to the ETC (ATP generation) have high expression at ZT19, whereas genes involved in lipid degradation (β-oxidation) show high expression at ZT0 and ZT2 in RPE cells. These data suggest that the highest energy demand of RPE cells is at night, when they use glycogen and glucose but not FAs as an energy source. Additionally, our data suggest that POS phagocytosis might be facilitated by cholesterol synthesis in the morning. Moreover, it has been suggested that the degradation of POSs is facilitated by FA degradation, which also takes place in the morning. Furthermore, we identified genes involved in lipid synthesis that are upregulated at night, possibly playing a role in generating building blocks for membrane synthesis. Although recycling of FAs from the RPE to PR cells has been identified previously,[53] future research is needed to determine whether these building blocks are used by the RPE itself or transported to the PR cells to generate POSs.

Acknowledgments

The authors thank Niky Thijssen for her expert technical assistance and Andries Kalsbeek of the Netherlands Institute for Neuroscience for critically reviewing our manuscript.

Supported by a junior researcher grant from the Radboud Institute for Molecular Life Sciences and Radboud University Medical Center, The Netherlands.

Disclosure: **E.M.M. Louer**, None; **G. Yi**, None; **C. Carmone**, None; **J. Robben**, None; **H.G. Stunnenberg**, None; **A.I. den Hollander**, None; **P.M.T. Deen**, None

References

1. Kenyon E, Yu K, La Cour M, Miller SS. Lactate transport mechanisms at apical and basolateral membranes of bovine retinal pigment epithelium. *Am J Physiol*. 1994;267:C1561–C1573.
2. la Cour M, Lin H, Kenyon E, Miller SS. Lactate transport in freshly isolated human fetal retinal pigment epithelium. *Invest Ophthalmol Vis Sci*. 1994;35:434–442.
3. Young RW, Bok D. Participation of the retinal pigment epithelium in the rod outer segment renewal process. *J Cell Biol*. 1969;42:392–403.
4. Palczewski K, Baehr W. The retinoid cycle and retinal diseases. *eLS*. 2001;doi: 10.1038/npg.els.0004067.
5. Strauss O. The retinal pigment epithelium in visual function. *Physiol Rev*. 2005;85:845–881.
6. Gordon WC, Bazan NG. Visualization of [3H] docosahexaenoic acid trafficking through photoreceptors and retinal pigment epithelium by electron microscopic autoradiography. *Invest Ophthalmol Vis Sci*. 1993;34:2402–2411.
7. Adler AJ, Southwick RE. Distribution of glucose and lactate in the interphotoreceptor matrix. *Ophthalmic Res*. 1992;24:243–252.
8. Young RW. The renewal of photoreceptor cell outer segments. *J Cell Biol*. 1967;33:61–72.
9. Chen H, Anderson RE. Metabolism in frog retinal pigment epithelium of docosahexaenoic and arachidonic acids derived from rod outer segment membranes. *Exp Eye Res*. 1993;57:369–377.
10. Tyni T, Johnson M, Eaton S, et al. Mitochondrial fatty acid β-oxidation in the retinal pigment epithelium. *Pediatr Res*. 2002;52:595–600.
11. Tyni T, Paetau A, Strauss AW, Middleton B, Kivelä T. Mitochondrial fatty acid β-oxidation in the human eye and brain: implications for the retinopathy of long-chain 3-hydroxyacyl-CoA dehydrogenase deficiency. *Pediatr Res*. 2004;56:744–750.
12. LaVail MM. Rod outer segment disc shedding in relation to cyclic lighting. *Exp Eye Res*. 1976;23:277–280.
13. LaVail M. Circadian nature of rod outer segment disc shedding in the rat. *Invest Ophthalmol Vis Sci*. 1980;19:407–411.
14. Ruggiero L, Connor MP, Chen J, Langen R, Finnemann SC. Diurnal, localized exposure of phosphatidylserine by rod outer segment tips in wild-type but not Itgb5–/– or Mfge8–/– mouse retina. *Proc Natl Acad Sci U S A*. 2012;109:8145–8148.
15. Nandrot EF, Anand M, Sircar M, Finnemann SC. Novel role for alphavbeta5-integrin in retinal adhesion and its diurnal peak. *Am J Physiol Cell Physiol*. 2006;290:C1256–C1262.
16. Handa JT. How does the macula protect itself from oxidative stress? *Mol Aspects Med*. 2012;33:418–435.
17. Nowak JZ. Oxidative stress, polyunsaturated fatty acids-derived oxidation products and bisretinoids as potential inducers of CNS diseases: focus on age-related macular degeneration. *Pharmacol Rep*. 2013;65:288–304.
18. Dobin A, Davis CA, Schlesinger F, et al. STAR: ultrafast universal RNA-seq aligner. *Bioinformatics*. 2013;29:15–21.
19. Newman AM, Liu CL, Green MR, et al. Robust enumeration of cell subsets from tissue expression profiles. *Nat Methods*. 2015;12:453–457.
20. Bennis A, Gorgels TG, Ten Brink JB, et al. Comparison of mouse and human retinal pigment epithelium gene expression profiles: potential implications for age-related macular degeneration. *PLoS One*. 2015;10:e0141597.
21. Love MI, Huber W, Anders S. Moderated estimation of fold change and dispersion for RNA-seq data with DESeq2. *Genome Biol*. 2014;15:550.
22. Trapnell C, Williams BA, Pertea G, et al. Transcript assembly and quantification by RNA-Seq reveals unannotated transcripts and isoform switching during cell differentiation. *Nat Biotechnol*. 2010;28:511–515.
23. Kuleshov MV, Jones MR, Rouillard AD, et al. Enrichr: a comprehensive gene set enrichment analysis web server 2016 update. *Nucleic Acids Res*. 2016;44:W90–W97.
24. Chen EY, Tan CM, Kou Y, et al. Enrichr: interactive and collaborative HTML5 gene list enrichment analysis tool. *BMC Bioinformatics*. 2013;14:128.
25. Kelder T, van Iersel MP, Hanspers K, et al. WikiPathways: building research communities on biological pathways. *Nucleic Acids Res*. 2012;40:D1301–D1307.

Investigative Ophthalmology & Visual Science

26. Kutmon M, Riutta A, Nunes N, et al. WikiPathways: capturing the full diversity of pathway knowledge. *Nucleic Acids Res*. 2016;44:D488–D494.
27. van Iersel MP, Kelder T, Pico AR, et al. Presenting and exploring biological pathways with PathVisio. *BMC Bioinformatics*. 2008;9:399.
28. Kutmon M, van Iersel MP, Bohler A, et al. PathVisio 3: an extendable pathway analysis toolbox. *PLoS Comput Biol*. 2015;11:e1004085.
29. Edgar R, Domrachev M, Lash AE. Gene Expression Omnibus: NCBI gene expression and hybridization array data repository. *Nucleic Acids Res*. 2002;30:207–210.
30. Zhang R, Lahens NF, Ballance HI, Hughes ME, Hogenesch JB. A circadian gene expression atlas in mammals: implications for biology and medicine. *Proc Natl Acad Sci USA*. 2014;111:16219–16224.
31. Gabriel JL, Zervos PR, Plaut GWE. Activity of purified NAD-specific isocitrate dehydrogenase at modulator and substrate concentrations approximating conditions in mitochondria. *Metabolism*. 1986;35:661–667.
32. Bonora M, Patergnani S, Rimessi A, et al. ATP synthesis and storage. *Purinergic Signal*. 2012;8:343–357.
33. Berg JM, Tymoczko JL, Stryer L. *Biochemistry*. 5th ed. New York, NY: W.H. Freeman; 2002.
34. Dzeja PP, Terzic A. Phosphotransfer networks and cellular energetics. *J Exp Biol*. 2003;206:2039–2047.
35. Sazanov LA. A giant molecular proton pump: structure and mechanism of respiratory complex I. *Nat Rev Mol Cell Biol*. 2015;16:375–388.
36. Swarup A, Samuels IS, Bell BA, et al. Modulating GLUT1 expression in the RPE decreases glucose levels in the retina: impact on photoreceptors and Müller glial cells. *Am J Physiol Cell Physiol*. 2018;316:C121–C133.
37. Coffe V, Carbajal RC, Salceda R. Glucose metabolism in rat retinal pigment epithelium. *Neurochem Res*. 2006;31:103–108.
38. Golestaneh N, Chu Y, Xiao YY, Stoleru GL, Theos AC. Dysfunctional autophagy in RPE, a contributing factor in age-related macular degeneration. *Cell Death Dis*. 2017;8:e2537.
39. Hernandez C, Garcia-Ramirez M, Garcia-Rocha M, et al. Glycogen storage in the human retinal pigment epithelium: a comparative study of diabetic and non-diabetic donors. *Acta Diabetol*. 2014;51:543–552.
40. Elsbach P, Levy S. Increased synthesis of phospholipid during phagocytosis. *J Clin Invest*. 1968;47:2217–2229.
41. Goepfert S, Poirier Y. Beta-oxidation in fatty acid degradation and beyond. *Curr Opin Plant Biol*. 2007;10:245–251.
42. Adijanto J, Du J, Moffat C, et al. The retinal pigment epithelium utilizes fatty acids for ketogenesis. *J Biol Chem*. 2014;289:20570–20582.
43. Reyes-Reveles J, Dhingra A, Alexander D, et al. Phagocytosis-dependent ketogenesis in retinal pigment epithelium. *J Biol Chem*. 2017;292:8038–8047.
44. Chao JR, Knight K, Engel AL, et al. Human retinal pigment epithelial cells prefer proline as a nutrient and transport metabolic intermediates to the retinal side. *J Biol Chem*. 2017;292:12895–12905.
45. Storti F, Raphael G, Griesser V, et al. Regulated efflux of photoreceptor outer segment-derived cholesterol by human RPE cells. *Exp Eye Res*. 2017;165:65–77.
46. Kusumi A, Tsuda M, Akino T, Ohnishi S, Terayama Y. Protein-phospholipid-cholesterol interaction in the photolysis of invertebrate rhodopsin. *Biochemistry*. 1983;22:1165–1170.
47. Dorey CK, Wu G, Ebenstein D, Garsd A, Weiter JJ. Cell loss in the aging retina. Relationship to lipofuscin accumulation and macular degeneration. *Invest Ophthalmol Vis Sci*. 1989;30:1691–1699.
48. Miceli MV, Liles MR, Newsome DA. Evaluation of oxidative processes in human pigment epithelial cells associated with retinal outer segment phagocytosis. *Exp Cell Res*. 1994;214:242–249.
49. Jarrett SG, Lewin AS, Boulton ME. The importance of mitochondria in age-related and inherited eye disorders. *Ophthalmic Res*. 2010;44:179–190.
50. Schutt F, Aretz S, Auffarth GU, Kopitz J. Moderately reduced ATP levels promote oxidative stress and debilitate autophagic and phagocytic capacities in human RPE cells. *Invest Ophthalmol Vis Sci*. 2012;53:5354–5361.
51. He Y, Tombran-Tink J. Mitochondrial decay and impairment of antioxidant defenses in aging RPE cells. *Adv Exp Med Biol*. 2010;664:165–183.
52. Rohrer B, Bandyopadhyay M, Beeson C. Reduced metabolic capacity in aged primary retinal pigment epithelium (RPE) is correlated with increased susceptibility to oxidative stress. *Adv Exp Med Biol*. 2016;854:793–798.
53. Chen H, Wiegand RD, Koutz CA, Anderson RE. Docosahexaenoic acid increases in frog retinal pigment epithelium following rod photoreceptor shedding. *Exp Eye Res*. 1992;55:93–100.

Investigative Ophthalmology & Visual Science